Vietnam Journal of Mechanics, VAST, Vol. 43, No. 3 (2021), pp. 277 – 295
DOI: https://doi.org/10.15625/0866-7136/15981

FREE VIBRATION AND BUCKLING OF BIDIRECTIONAL FUNCTIONALLY GRADED SANDWICH PLATES USING AN EFFICIENT Q9 ELEMENT

Cong Ich Le[1,*], Quang Dung Tran[1], Vu Nam Pham[2,3], Dinh Kien Nguyen[3,4]
[1]*Le Quy Don Technical University, 236 Hoang Quoc Viet, Hanoi, Vietnam*
[2]*Thuyloi University, 175 Tay Son, Dong Da, Hanoi, Vietnam*
[3]*Graduate University of Science and Technology, VAST, 18 Hoang Quoc Viet, Hanoi, Vietnam*
[4]*Institute of Applied Mechanics, VAST, Hanoi, Vietnam*
[*]E-mail: lecongich79@lqdtu.edu.vn

Received: 05 April 2021 / Published online: 18 July 2021

Abstract. Free vibration and buckling of three-phase bidirectional functionally graded sandwich (BFGSW) plates are studied in this paper for the first time by using an efficient nine-node quadrilateral (Q9) element. The core of the sandwich plates is pure ceramic, while the two skin layers are of a three-phase bidirectional functionally graded material. The element is derived on the basis of the Mindlin plate theory and linked interpolations. Fundamental frequencies and buckling loads are computed for the plates with various boundary conditions. Numerical result shows that convergence of the linked interpolation element is faster compared to the conventional Lagrangian interpolation Q9 element. Numerical investigations are carried out to highlight the influence of the material gradation and the side-to-thickness ratio on the vibration and buckling behaviour of the plates.

Keywords: BFGSW plate, Q9 element, linked interpolation, vibration and buckling analysis.

1. INTRODUCTION

Functionally graded materials (FGMs) with outstanding properties compared to conventional composites in term of reducing thermal stresses are increasingly employed to fabricate structural elements for use in severe conditions. Study on mechanical behaviour of FGM structures subjected to different thermal and mechanical loadings is the subject of investigations in the last few decades [1,2]. Recently, thanks to the advanced manufacturing methods [3], the use of FGMs in sandwich construction for improving structural performance and overcoming the inter-layer delaminating problems of conventional sandwich structures has been realized. Functionally graded sandwich (FGSW) structures with high stiffness-to-weight ratio and continuous variation of material properties are widely used in many modern engineering applications such as aerospace, marine and nuclear

energy engineering. Analyses of FGSW structures in general, FGSW plates in particular are extensively carried out, contributions that are most relevant to present work are briefly discussed below.

Bending, vibration and buckling analyses of sandwich plates with a homogeneous core and transversely FGM faces were carried out by Zenkour [4, 5] on the basis of different plate theories. The influence of the material distribution, aspect ratio and relative ratio of the core to the plate thickness on the behaviour of the plates was examined in detail in the works. Thermal buckling loads of a FGSW plate was evaluated in [6] via the sinusoidal shear deformation theory. Li et al. [7] studied free vibration FGSW rectangular plates on the basis of a three-dimensional linear theory of elasticity. The plate displacements have been expanded into series of Chebyshev polynomials and the Ritz method was used to obtain the vibration characteristics. Xiang et al. [8, 9] calculated natural frequencies of sandwich plates with homogeneous core and FGM face sheets using the n-order shear deformation theory in combination with the meshless global collocation method. Neves et al. [10] presented a quasi-3D shear deformation theory for analyzing isotropic and FGSW plates, taking into account the extensibility in the thickness direction. The collocation with radial basis functions was adopted by the authors to obtain the static, buckling, and free vibration characteristics. The bending, buckling, and free vibration of FGSW plates were investigated by Thai et al. [11–13], using the new first-order and higher-order shear deformation theories. Results obtained by the authors were compared with 3D and quasi-3D solutions and those predicted by other plate theories. The refined zigzag theory was adopted by Iurlaro et al. [14] in formulating finite element formulations for bending and free vibration analysis of FGSW plates. Numerical investigations by the authors showed that the zigzag theory is superior to the first-order and third-order shear deformation theories in predicting the mechanical behavior of the plates. Pandey and Pradyumna [15] employed the higher-order layerwise theory to derive an eight-node isoparametric element for static and dynamic analyses of FGSW plates. The efficiency and accuracy of the element in evaluating bending and dynamic characteristics of the plates were confirmed through a numerical study. Free vibration analysis of FGSW plate was carried out by Belabed et al. [16] using a hyperbolic plate theory. The influence of porosities on bending behaviour of a sandwich plate with a homogeneous core and FGM face layers was studied by Daikh and Zenkour [17], using a high-order shear deformation theory. The quasi-3D shear deformation theory, taking into account the thickness stretching effect, was adopted by by Le et al. [18] in formulating a finite element formulation for computing natural frequencies and mode shapes of FGSW plates partially supported by a Pasternak foundation.

Development of FGM structures with properties varying in two or more directions to withstand complex loading is of practical demand [19]. Due to the coefficients of governing equations for bidirectional FGM (BFGM) plates varying in the longitudinal direction, analytical methods is often difficult in dealing with BFGM plates. Development of efficient finite element formulations, therefore is important in analysis of BFGM plates. In addition, the concept of linked interpolation, which has been put forward by Zienkiewicz et al. [20] in formulating a Mindlin plate element, leads to a simple, but efficient plate element. The concept can be easily extended to a triangle for bending analysis of both thin

and thick plates [21]. An alternative quadrilateral element for Reissner-Mindlin plates, extended the mixed formulation described in [20] was presented by Xu et al. [22], using the linked interpolations. Different from the linear quadrilateral element in [20], the element in [22] used four internal rotation nodes and a linear approximation for transverse shear forces. It was shown that the element passed various patch tests, did not possess any zero-energy mode, and its performance was good for both thick and thin plates. Higher-order linked interpolation quadrilateral and triangular elements for thick homogeneous plate was derived by Ribaric [23, 24]. It was shown that the higher-order elements, in general, are successful compared to lower-order elements in the problems with the same total number of the degrees of freedom.

In this paper, vibration and buckling analysis of three-phase bidirectional functionally graded sandwich (BFGSW) plates is studied for the first time by using a nine-node quadrilateral (Q9) element. To the authors' best knowledge, this problem has not been reported in the literature, and thus it is studied herein for the first time. The plates consist of three layers, a pure ceramic core and two face sheets of three-phase BFGM. The material properties of the face sheets are considered to vary in both the plate thickness and length by power gradation laws. In order to improve the element performance, the linked interpolations are employed in the derivation of the element stiffness and mass matrices. Using the derived element, frequencies and buckling loads are computed for the plates with various boundary conditions. The effects of material distribution and the layer thickness ratio on the frequencies and buckling loads are studied and highlighted. The influence of the side-to-thickness ratio on the behaviour of the plates is also examined and discussed.

2. BFGSW PLATE

A rectangular BFGSW plate with length a, width b and thickness h, as depicted in Fig. 1, is considered. The Cartesian system (x, y, z) in the figure is chosen such that the

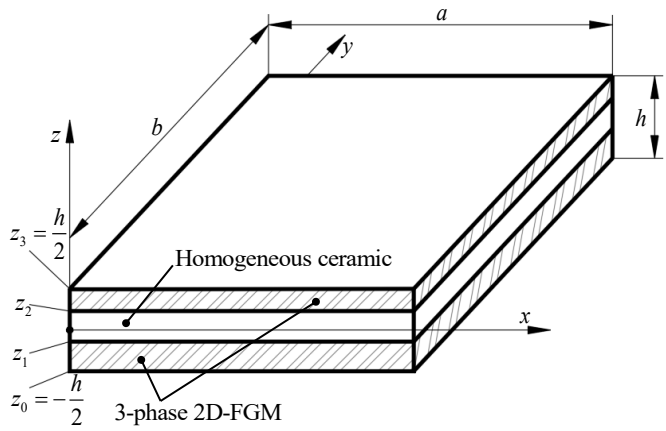

Fig. 1. A rectangular BFGSW plate: geometry and coordinates

(x, y) plane is coincident with the mid-plane, and z-axis directs upward. The plate consists of three layers, a homogeneous ceramic core and two FGM skin layers. Denoting $z_0 = -h/2$, z_1, z_2 and $z_3 = h/2$ are, respectively, the vertical coordinates of the bottom surface, the interfaces between the layers, and the top surface. The FGM layers are made from three constituents, M1, M2 and M3, with volume fraction smoothly varying in both the x- and z-directions according to [25,26]

$$\begin{cases} V_1 = \left(\dfrac{z - z_0}{z_1 - z_0}\right)^{n_z}, \\ V_2 = \left[1 - \left(\dfrac{z - z_0}{z_1 - z_0}\right)^{n_z}\right]\left[1 - \left(\dfrac{x}{a}\right)^{n_x}\right], & \text{for } z \in [z_0,\ z_1] \\ V_3 = \left[1 - \left(\dfrac{z - z_0}{z_1 - z_0}\right)^{n_z}\right]\left(\dfrac{x}{a}\right)^{n_x}, \end{cases}$$
$$V_1 = 1, V_2 = V_3 = 0, \qquad \text{for } z \in [z_1,\ z_2] \tag{1}$$
$$\begin{cases} V_1 = \left(\dfrac{z - z_3}{z_2 - z_3}\right)^{n_z}, \\ V_2 = \left[1 - \left(\dfrac{z - z_3}{z_2 - z_3}\right)^{n_z}\right]\left[1 - \left(\dfrac{x}{a}\right)^{n_x}\right], & \text{for } z \in [z_2,\ z_3] \\ V_3 = \left[1 - \left(\dfrac{z - z_3}{z_2 - z_3}\right)^{n_z}\right]\left(\dfrac{x}{a}\right)^{n_x}, \end{cases}$$

where V_1, V_2, and V_3 are, respectively, the volume fraction of M1, M2, and M3; n_x and n_z are the axial and transverse power-law indexes. It is easy to verify that if $n_x = 0$ or M2 is identical to M3, Eq. (1) returns to volume fraction of the conventional two-phase FGM sandwich plates in [5,13,27]. The thickness and longitudinal distribution of V_1, V_2 and V_3 is shown in Fig. 2 for a (2-2-1) plate with $n_x = 0.5$, $n_z = 1$ and $z_1 = -h/10$, $z_2 = 3h/10$. Noting that the three number in brackets are used herein to denote the layer thickness ratio, e.g. (2-2-1) means that the thickness ratio of the bottom, core and the top layers is $2 : 2 : 1$.

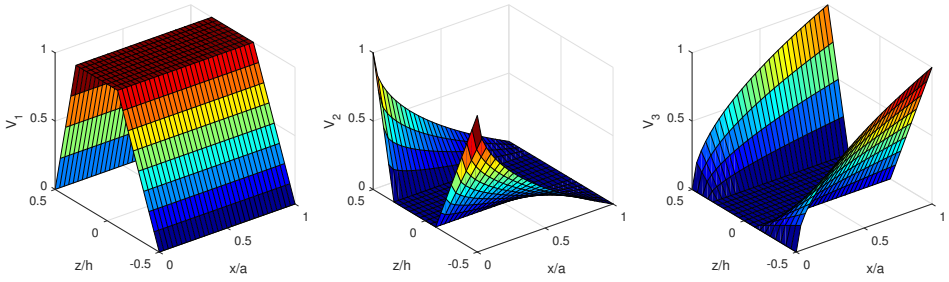

Fig. 2. Distribution of V_1, V_2, and V_3 for $n_x = 0.5$, $n_z = 1$ and $z_1 = -h/10$, $z_2 = 3h/10$

The effective property (P) such as elastic modulus and mass density of the BFGM skin layers evaluated by the Voigt's model is of the form

$$P(x,z) = V_1 P_1 + V_2 P_2 + V_3 P_3, \tag{2}$$

with P_1, P_2, and P_3 are the properties of the M1, M2 and M3, respectively.

Substituting (1) into (2), one gets

$$P(x,z) = \begin{cases} [P_1 - P_{23}(x)] \left(\dfrac{z - z_0}{z_1 - z_0}\right)^{n_z} + P_{23}(x), & \text{for } z \in [z_0,\ z_1] \\ P_1, & \text{for } z \in [z_1,\ z_2] \\ [P_1 - P_{23}(x)] \left(\dfrac{z - z_3}{z_2 - z_3}\right)^{n_z} + P_{23}(x), & \text{for } z \in [z_2,\ z_3] \end{cases} \tag{3}$$

where

$$P_{23}(x) = P_2 - (P_2 - P_3) \left(\frac{x}{a}\right)^{n_x}, \tag{4}$$

3. MATHEMATICAL FORMULATION

Based on Mindlin plate theory [28], the displacements of a point in x, y and z directions, $u(x,y,z,t)$, $v(x,y,z,t)$ and $w(x,y,z,t)$, respectively, are given by

$$\begin{aligned} u(x,y,z,t) &= u_0(x,y,t) + z\beta_x(x,y,t), \\ v(x,y,z,t) &= v_0(x,y,t) + z\beta_y(x,y,t), \\ w(x,y,z,t) &= w_0(x,y,t), \end{aligned} \tag{5}$$

where $u_0(x,y,t)$, $v_0(x,y,t)$ and $w_0(x,y,t)$ are, respectively, the in-plane and transverse displacements of a point on the mid-plane; β_x and β_y are the rotations around the y-axis and x-axis of a mid-plane normal, respectively. The positive directions of the displacements and rotations are shown in Fig. 3.

Eq. (5) gives the strains in the forms

$$\boldsymbol{\varepsilon}_b = \begin{Bmatrix} \varepsilon_x \\ \varepsilon_y \\ \gamma_{xy} \end{Bmatrix} = \begin{Bmatrix} \varepsilon_x^0 \\ \varepsilon_y^0 \\ \gamma_{xy}^0 \end{Bmatrix} + z \begin{Bmatrix} \kappa_x \\ \kappa_y \\ \kappa_{xy} \end{Bmatrix} = \boldsymbol{\varepsilon}^0 + z\boldsymbol{\kappa}, \quad \boldsymbol{\gamma}_s = \begin{Bmatrix} \gamma_{xz} \\ \gamma_{yz} \end{Bmatrix} = \begin{Bmatrix} w_{0,x} + \beta_x \\ w_{0,y} + \beta_y \end{Bmatrix}, \tag{6}$$

where $\boldsymbol{\varepsilon}_b$ and $\boldsymbol{\gamma}_s$ are, respectively, the vectors of bending and shear strains, and

$$\begin{aligned} &\varepsilon_x^0 = u_{0,x},\ \varepsilon_y^0 = v_{0,y},\ \gamma_{xy}^0 = u_{0,y} + v_{0,x}, \\ &\kappa_x = \beta_{x,x},\ \kappa_y = \beta_{y,y},\ \kappa_{xy} = \beta_{x,y} + \beta_{y,x}. \end{aligned} \tag{7}$$

In the above equation and hereafter, a subscript comma is used to denote the derivative with respect to the followed variable, e.g. $w_{0,x} = \partial w_0 / \partial x$.

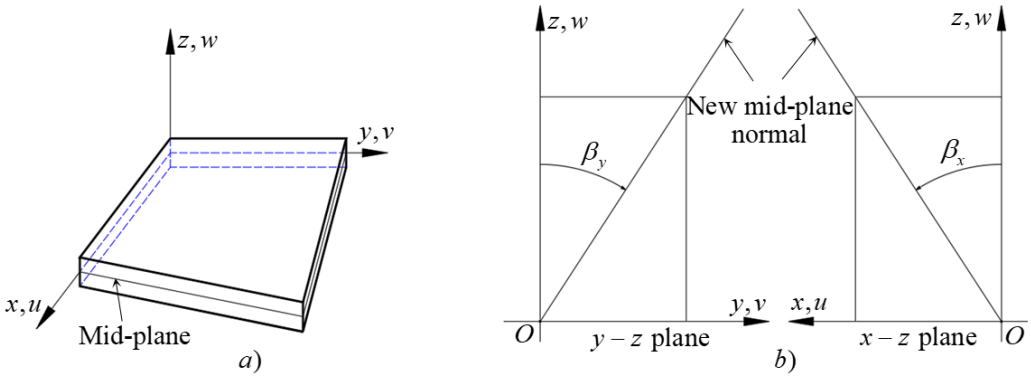

Fig. 3. Positive directions of u, v, w displacements (a) and rotations β_x and β_y of a quadrilateral Mindlin plate element

Constitutive equations based on linear assumption of the material behaviour are

$$\boldsymbol{\sigma}_b = \begin{Bmatrix} \sigma_x \\ \sigma_y \\ \tau_{xy} \end{Bmatrix} = \begin{bmatrix} Q_{11} & Q_{12} & 0 \\ Q_{12} & Q_{11} & 0 \\ 0 & 0 & Q_{22} \end{bmatrix} \begin{Bmatrix} \varepsilon_x \\ \varepsilon_y \\ \gamma_{xy} \end{Bmatrix} = \mathbf{D}_b \boldsymbol{\varepsilon}_b, \tag{8}$$

$$\boldsymbol{\tau}_s = \begin{Bmatrix} \tau_{xz} \\ \tau_{yz} \end{Bmatrix} = \psi \begin{bmatrix} Q_{22} & 0 \\ 0 & Q_{22} \end{bmatrix} \begin{Bmatrix} \gamma_{xz} \\ \gamma_{yz} \end{Bmatrix} = \mathbf{D}_s \boldsymbol{\gamma}_s, \tag{9}$$

where $Q_{11}(x,z) = \dfrac{E(x,z)}{(1-\nu^2)}$; $Q_{12}(x,z) = \nu Q_{11}(x,z)$; $Q_{22}(x,z) = \dfrac{E(x,z)}{2(1+\nu)}$ with Young's modulus $E(x,z)$ is defined by Eqs. (3) and Poison's ratio ν is assumed to be constant. The shear correction factor ψ in (9) is chosen by 5/6 for the present plate.

Eqs. (6), (8) and (9) give the strain energy $\mathcal{U}$ in the form

$$\mathcal{U} = \frac{1}{2}\int_V \begin{Bmatrix} \boldsymbol{\sigma}_b \\ \boldsymbol{\tau}_s \end{Bmatrix}^T \begin{Bmatrix} \boldsymbol{\varepsilon}_b \\ \boldsymbol{\gamma}_s \end{Bmatrix} \mathrm{d}V = \frac{1}{2}\int_0^a \int_0^b \begin{Bmatrix} \boldsymbol{\varepsilon}^0 \\ \boldsymbol{\kappa} \\ \boldsymbol{\gamma}_s \end{Bmatrix}^T \begin{bmatrix} \mathbf{I_1} & \mathbf{I_2} & 0 \\ \mathbf{I_2} & \mathbf{I_3} & 0 \\ 0 & 0 & \mathbf{I_4} \end{bmatrix} \begin{Bmatrix} \boldsymbol{\varepsilon}^0 \\ \boldsymbol{\kappa} \\ \boldsymbol{\gamma}_s \end{Bmatrix} \mathrm{d}x\mathrm{d}y, \tag{10}$$

where V is the plate volume; $\mathbf{I}_1$, $\mathbf{I}_2$, $\mathbf{I}_3$ and $\mathbf{I}_4$ are the matrices of the plate rigidities, defined as

$$(\mathbf{I_1}, \mathbf{I_2}, \mathbf{I_3}) = \int_{-h/2}^{h/2} \mathbf{D}_b(x,z)[1, z, z^2]\mathrm{d}z, \quad \mathbf{I_4} = \int_{-h/2}^{h/2} \mathbf{D}_s(x,z)\mathrm{d}z. \tag{11}$$

In Eq. (10) and hereafter a superscript 'T' denotes the transpose of a vector or a matrix. Using the technique in Ref. [26], explicit expressions for the rigidities in the above equation (and the mass moments in Eq. (13) also) can be obtained.

The kinetic energy of the plate resulted from Eq. (5) is of the form

$$\begin{aligned}\mathcal{T} &= \frac{1}{2}\int_V \rho(x,y,z)\{\dot{u}^2+\dot{v}^2+\dot{w}^2\}\mathrm{d}V \\ &= \frac{1}{2}\int_0^a\int_0^b \begin{Bmatrix}\dot{u}_0\\ \dot{v}_0\\ \dot{w}_0\\ \dot{\beta}_x\\ \dot{\beta}_y\end{Bmatrix}^T \begin{bmatrix}J_1 & 0 & 0 & J_2 & 0\\ 0 & J_1 & 0 & 0 & J_2\\ 0 & 0 & J_1 & 0 & 0\\ J_2 & 0 & 0 & J_3 & 0\\ 0 & J_2 & 0 & 0 & J_3\end{bmatrix} \begin{Bmatrix}\dot{u}_0\\ \dot{v}_0\\ \dot{w}_0\\ \dot{\beta}_x\\ \dot{\beta}_y\end{Bmatrix} \mathrm{d}x\mathrm{d}y,\end{aligned} \tag{12}$$

where an over dot denotes the derivative with respect to the time variable t, and the mass moments $J_1,\ J_2,\ J_3$ are defined as

$$(J_1,\ J_2,\ J_3) = \int_{-h/2}^{h/2}\rho(x,z)[1,z,z^2]\mathrm{d}z. \tag{13}$$

Finally, the potential energy resulted by the in-plane load (P_x^0, P_y^0, P_{xy}^0) is of the form

$$\begin{aligned}\mathcal{V} &= \frac{1}{2}\int_0^a\int_0^b (P_x^0\, w_{0,x}^2 + P_y^0\, w_{0,y}^2 + 2P_{xy}^0\, w_{0,xy}^2)\mathrm{d}x\mathrm{d}y \\ &= \frac{1}{2}\int_0^a\int_0^b \begin{Bmatrix}w_{0,x}\\ w_{0,y}\\ w_{0,xy}\end{Bmatrix}^T \begin{bmatrix}P_x^0 & 0 & 0\\ 0 & P_y^0 & 0\\ 0 & 0 & 2P_{xy}^0\end{bmatrix} \begin{Bmatrix}w_{0,x}\\ w_{0,y}\\ w_{0,xy}\end{Bmatrix} \mathrm{d}x\mathrm{d}y,\end{aligned} \tag{14}$$

with (P_x^0, P_y^0, P_{xy}^0) are negative for compressive loads.

4. LINKED INTERPOLATION Q9 ELEMENT

Fig. 4(a) shows a typical mesh for finite element analysis of a rectangular plate obtained by an automatic meshing algorithm. A generic nine-node quadrilateral (Q9) element of the mesh in global and a natural coordinates, (x, y) and (ξ, η), respectively, is depicted in Fig. 4(b). In the figure, $(i.j),\ (i = 1 \div 3,\ j = 1 \div 3)$ are the nodes of the element; a_i and b_j are, respectively, the distances between the nodes in the ξ- and η-directions. The

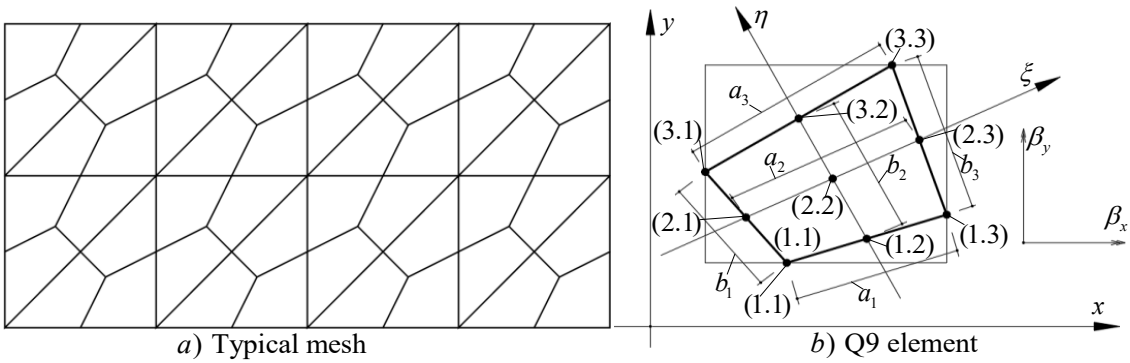

Fig. 4. A typical finite element mesh for plate (a), and Q9 element (b)

nodal displacements $u_0^{ij}, v_0^{ij}, w_0^{ij}, \beta_x^{ij}, \beta_y^{ij}$ are taken herein as element degrees of freedom. The vector of nodal displacements contains 46 components as

$$\underset{46\times 1}{\mathbf{d}_e} = \{\mathbf{d}_u \;\; \mathbf{d}_v \;\; \mathbf{d}_w \;\; \mathbf{d}_{\beta_x} \;\; \mathbf{d}_{\beta_y} \;\; w_b\}^T, \tag{15}$$

where $\mathbf{d}_u = \{u_0^{ij}\}$ is the vector of nodal displacements in x-direction; $\mathbf{d}_v$, $\mathbf{d}_w$, $\mathbf{d}_{\beta_x}$ and $\mathbf{d}_{\beta_y}$ are defined similarly as $\mathbf{d}_u$; w_b is an additional independent bubble degree of freedom.

The linked interpolation for the displacement w_0 over the whole element domain are given by [23]

$$\begin{aligned} w_0 &= \sum_{j=1}^{3}\sum_{i=1}^{3}\left(N_{ij}w_0^{ij} + N_{w\beta_x}^{ij}\beta_x^{ij} + N_{w\beta_y}^{ij}\beta_y^{ij}\right) + N_{w_b}w_b \\ &= \mathbf{N}\mathbf{d}_w + \mathbf{N}_{w\beta_x}\mathbf{d}_{\beta_x} + \mathbf{N}_{w\beta_y}\mathbf{d}_{\beta_y} + N_{w_b}w_b = \mathbf{N}_w\mathbf{d}_e, \end{aligned} \tag{16}$$

while the interpolation for u_0, v_0, β_x and β_y takes the standard Lagrangian form as

$$\begin{aligned} u_0 &= \sum_{j=1}^{3}\sum_{i=1}^{3} N_{ij}u_0^{ij} = \mathbf{N}\mathbf{d}_u = \mathbf{N}_u\mathbf{d}_e, \;\; v_0 = \sum_{j=1}^{3}\sum_{i=1}^{3} N_{ij}v_0^{ij} = \mathbf{N}\mathbf{d}_v = \mathbf{N}_v\mathbf{d}_e, \\ \beta_x &= \sum_{j=1}^{3}\sum_{i=1}^{3} N_{ij}\beta_x^{ij} = \mathbf{N}\mathbf{d}_{\beta_x} = \mathbf{N}_{\beta_x}\mathbf{d}_e, \;\; \beta_y = \sum_{j=1}^{3}\sum_{i=1}^{3} N_{ij}\beta_y^{ij} = \mathbf{N}\mathbf{d}_{\beta_y} = \mathbf{N}_{\beta_y}\mathbf{d}_e, \end{aligned} \tag{17}$$

where

$$\begin{aligned} &N_{ij} = I_{j\xi}I_{i\eta}, \;\; N_{w_b} = \frac{\xi I_{2\xi}}{4}\frac{\eta I_{2\eta}}{4}, \\ &N_{w\beta_x}^{ij} = (-1)^{j+1}a_i\cos\phi_{a_i}I_{i\eta}(\xi-\xi^3)k_j + (-1)^i b_j\cos\phi_{b_j}I_{j\xi}(\eta-\eta^3)k_i, \\ &N_{w\beta_y}^{ij} = (-1)^{j+1}a_i\sin\phi_{a_i}I_{i\eta}(\xi-\xi^3)k_j + (-1)^i b_j\sin\phi_{b_j}I_{j\xi}(\eta-\eta^3)k_i, \end{aligned} \tag{18}$$

with $I_{1\xi} = -\xi(1-\xi)/2$; $I_{2\xi} = 1-\xi^2$; $I_{3\xi} = \xi(1+\xi)/2$; $I_{1\eta}$, $I_{2\eta}$ and $I_{3\eta}$ are the corresponding interpolation functions with the natural coordinates ξ and η; $k_1 = k_3 = 1/12$; $k_2 = 1/6$; ϕ_{a_i} or ϕ_{b_j} is the angle that the normal to the edge makes with the x-axis, that is $\cos\phi_{a_i} = -(y_{i3}-y_{i1})/a_i$, $\sin\phi_{a_i} = (x_{i3}-x_{i1})/a_i$ and $\cos\phi_{b_j} = -(y_{1j}-y_{3j})/b_j$, $\sin\phi_{b_j} = (x_{1j}-x_{3j})/b_j$.

The matrices of interpolation $\mathbf{N}_u$, $\mathbf{N}_v$, $\mathbf{N}_w$, $\mathbf{N}_{\beta_x}$ and $\mathbf{N}_{\beta_y}$ (size of 1×46) in Eqs. (16), and (17) are of the forms

$$\begin{aligned} \mathbf{N}_u &= \{\mathbf{N} \;\; [0] \;\; [0] \;\; [0] \;\; [0] \;\; 0\}, \\ \mathbf{N}_v &= \{[0] \;\; \mathbf{N} \;\; [0] \;\; [0] \;\; [0] \;\; 0\}, \\ \mathbf{N}_w &= \{[0] \;\; [0] \;\; \mathbf{N} \;\; \mathbf{N}_{w\beta_x} \;\; \mathbf{N}_{w\beta_y} \;\; N_{w_b}\}, \\ \mathbf{N}_{\beta_x} &= \{[0] \;\; [0] \;\; [0] \;\; \mathbf{N} \;\; [0] \;\; 0\}, \\ \mathbf{N}_{\beta_y} &= \{[0] \;\; [0] \;\; [0] \;\; [0] \;\; \mathbf{N} \;\; 0\}. \end{aligned} \tag{19}$$

The relation between two coordinate systems (x, y) and (ξ, η) is as follows

$$\{x, y\} = \sum_{j=1}^{3}\sum_{i=1}^{3} N_{ij}\{x_{ij}, y_{ij}\} = \mathbf{N}\{\mathbf{X}^e, \mathbf{Y}^e\}, \tag{20}$$

with $\mathbf{X}^e = \{x_{ij}\}$, $\mathbf{Y}^e = \{y_{ij}\}$ (size 9×1) are the column vectors of the nodal global coordinates of the element. Noting that

$$\begin{Bmatrix} (.)_{,\xi} \\ (.)_{,\eta} \end{Bmatrix} = \begin{bmatrix} x_{,\xi} & y_{,\xi} \\ x_{,\eta} & y_{,\eta} \end{bmatrix} \begin{Bmatrix} (.)_{,x} \\ (.)_{,y} \end{Bmatrix} = \mathbf{J} \begin{Bmatrix} (.)_{,x} \\ (.)_{,y} \end{Bmatrix} \quad \text{or} \quad \begin{Bmatrix} (.)_{,x} \\ (.)_{,y} \end{Bmatrix} = \mathbf{J}^{-1} \begin{Bmatrix} (.)_{,\xi} \\ (.)_{,\eta} \end{Bmatrix}, \tag{21}$$

and $\mathrm{d}x\mathrm{d}y = \|\mathbf{J}\|\,\mathrm{d}\xi\mathrm{d}\eta$, with $\|\mathbf{J}\|$ is the determinant of Jacobian matrix.

Using the above interpolations, one can write the strain energy of the plate in Eq. (10) in the form

$$\mathcal{U} = \frac{1}{2}\sum^{\mathrm{NE}} \mathbf{d}_e^T \mathbf{k}_e\, \mathbf{d}_e, \tag{22}$$

where NE is the total number of elements; $\mathbf{k}_e$ is the element stiffness matrix, which can be written as

$$\underset{46\times46}{\mathbf{k}_e} = \int_{\Omega_e} \begin{Bmatrix} \mathbf{B}_{\prime\prime 0} \\ \mathbf{B}_{\check{}} \\ \mathbf{B}_{\mathbf{fl_s}} \end{Bmatrix}^T \begin{bmatrix} \mathbf{I_1} & \mathbf{I_2} & 0 \\ \mathbf{I_2} & \mathbf{I_3} & 0 \\ 0 & 0 & \mathbf{I_4} \end{bmatrix} \begin{Bmatrix} \mathbf{B}_{\prime\prime 0} \\ \mathbf{B}_{\check{}} \\ \mathbf{B}_{\mathbf{fl_s}} \end{Bmatrix} dxdy = \int_{\Omega_e} \mathbf{f}_K(x, y)\mathrm{d}x\mathrm{d}y, \tag{23}$$

with Ω_e is the area of the element domain, and

$$\underset{3\times46}{\mathbf{B}_{\varepsilon^0}} = \begin{Bmatrix} \mathbf{N}_{u,x} \\ \mathbf{N}_{v,y} \\ \mathbf{N}_{u,y} + \mathbf{N}_{v,x} \end{Bmatrix}, \quad \underset{3\times46}{\mathbf{B}_{\kappa}} = \begin{Bmatrix} \mathbf{N}_{\beta_x,x} \\ \mathbf{N}_{\beta_y,y} \\ \mathbf{N}_{\beta_x,y} + \mathbf{N}_{\beta_y,x} \end{Bmatrix}, \quad \underset{2\times46}{\mathbf{B}_{\gamma_s}} = \begin{Bmatrix} \mathbf{N}_{w,x} + \mathbf{N}_{\beta_x} \\ \mathbf{N}_{w,y} + \mathbf{N}_{\beta_y} \end{Bmatrix}. \tag{24}$$

The kinetic energy of the plate in Eq. (26) can also be written in the form

$$\mathcal{T} = \frac{1}{2}\sum^{NE} \mathbf{d}_e^T \mathbf{m}_e\, \mathbf{d}_e, \tag{25}$$

where $\mathbf{m}_e$ is the element mass matrix, which can be written in matrix form as

$$\underset{46\times46}{\mathbf{m}_e} = \int_{\Omega_e} \begin{Bmatrix} \mathbf{N}_u \\ \mathbf{N}_v \\ \mathbf{N}_w \\ \mathbf{N}_{\beta_x} \\ \mathbf{N}_{\beta_y} \end{Bmatrix}^T \begin{bmatrix} J_1 & 0 & 0 & J_2 & 0 \\ 0 & J_1 & 0 & 0 & J_2 \\ 0 & 0 & J_1 & 0 & 0 \\ J_2 & 0 & 0 & J_3 & 0 \\ 0 & J_2 & 0 & 0 & J_3 \end{bmatrix} \begin{Bmatrix} \mathbf{N}_u \\ \mathbf{N}_v \\ \mathbf{N}_w \\ \mathbf{N}_{\beta_x} \\ \mathbf{N}_{\beta_y} \end{Bmatrix} \mathrm{d}x\mathrm{d}y = \int_{\Omega_e} \mathbf{f}_M(x, y)\mathrm{d}x\mathrm{d}y. \tag{26}$$

The potential energy $\mathcal{V}$ in Eq. (14) is now of the form

$$\mathcal{V} = \frac{1}{2}\sum^{NE} \mathbf{d}_e^T \mathbf{k}_e^G\, \mathbf{d}_e, \tag{27}$$

with $\mathbf{k}_e^G$ is the element geometric stiffness matrix with the following forms

$$\begin{aligned}\underset{46\times46}{\mathbf{k}_e^G} &= \int_{\Omega_e} (\mathbf{N}_{w,x}^T P_x^0 \mathbf{N}_{w,x} + \mathbf{N}_{w,y}^T P_y^0 \mathbf{N}_{w,y} + 2\,\mathbf{N}_{w,xy}^T P_{xy}^0 \mathbf{N}_{w,xy}) \mathrm{d}x\mathrm{d}y \\ &= \int_{\Omega_e} \begin{Bmatrix} \mathbf{N}_{w,x} \\ \mathbf{N}_{w,y} \\ \mathbf{N}_{w,xy} \end{Bmatrix}^T \begin{bmatrix} P_x^0 & 0 & 0 \\ 0 & P_y^0 & 0 \\ 0 & 0 & 2P_{xy}^0 \end{bmatrix} \begin{Bmatrix} \mathbf{N}_{w,x} \\ \mathbf{N}_{w,y} \\ \mathbf{N}_{w,xy} \end{Bmatrix} \mathrm{d}x\mathrm{d}y = \int_{\Omega_e} \mathbf{f}_G(x,y) \mathrm{d}x\mathrm{d}y. \end{aligned} \tag{28}$$

In terms of the natural coordinates, the above matrices $\mathbf{k}_e$, $\mathbf{m}_e$ and $\mathbf{k}_e^G$ take the forms

$$\begin{aligned} \mathbf{k}_e &= \int_{-1}^{1}\int_{-1}^{1} \mathbf{f}_K(x(\xi,\eta), y(\xi,\eta)) \left\|\mathbf{J}\right\| \mathrm{d}\xi\mathrm{d}\eta, \\ \mathbf{m}_e &= \int_{-1}^{1}\int_{-1}^{1} \mathbf{f}_M(x(\xi,\eta), y(\xi,\eta)) \left\|\mathbf{J}\right\| \mathrm{d}\xi\mathrm{d}\eta, \\ \mathbf{k}_e^G &= \int_{-1}^{1}\int_{-1}^{1} \mathbf{f}_G(x(\xi,\eta), y(\xi,\eta)) \left\|\mathbf{J}\right\| \mathrm{d}\xi\mathrm{d}\eta. \end{aligned} \tag{29}$$

Gauss quadrature with 6×6 points along the ξ- and η-directions is employed to evaluate the integrals in Eq. (29). More points have been used, but no improvement in the numerical results was seen.

Hamilton's principle applied to the plate is of the form

$$\delta \int_{t_1}^{t_2} (\mathcal{T} - \mathcal{U} - \mathcal{V})\, \mathrm{d}t = 0. \tag{30}$$

By assuming a harmonic form for the vector of nodal displacements, the Hamilton's principle leads to the following discrete equation of motion

$$(\mathbf{K} - P_{cr}\mathbf{K}^{\mathrm{G}} - \omega^2\mathbf{M})\bar{\mathbf{D}} = 0, \tag{31}$$

where $\mathbf{M}$, $\mathbf{K}$ and $\mathbf{K}^{\mathrm{G}}$ are, respectively, the global mass, stiffness and geometric matrices; P_{cr}, ω and $\bar{\mathbf{D}}$ are the critical buckling load, the frequency and the eigenvector of nodal displacements corresponding to an eigenvalue, respectively.

5. NUMERICAL INVESTIGATION

Numerical investigation is carried out in this section to show the accuracy and performance of the derived Q9 element as well as the influence of the material distribution and plate geometry on the vibration and buckling behaviour. Otherwise stated, a BFGSW plate made from alumina (Al_2O_3) as M1, stainless steel (SUS304) as M2, and aluminum (Al) as M3 is considered. The properties of these constituents are given in Table 1 [26].

Table 1. Properties of constituent materials of BFGSW plate

Materials	Role	E (GPa)	ρ (kg/m^3)	ν
Alumina (Al_2O_3)	M1	380	3800	0.3
Steel (SUS304)	M2	210	7800	0.3
Aluminum (Al)	M3	70	2707	0.3

Three types of boundary conditions (B.C.), namely simply supported at all edges (SSSS), simply supported at two longer edges and clamped at the others (SCSC), and clamped at all edges (CCCC), are considered. The constraints for these boundaries are as follows:

- $u_0 = w_0 = \beta_y = 0$ at $x = 0, a$; $v_0 = w_0 = \beta_x = 0$ at $y = 0, b$ for SSSS.
- $u_0 = v_0 = w_0 = \beta_x = \beta_y = 0$ at all edges for CCCC.
- $v_0 = w_0 = \beta_x = 0$ at $y = 0, b$; $u_0 = v_0 = w_0 = \beta_x = \beta_y = 0$ at $x = 0, a$ for SCSC.

For the convenience of discussion, the following non-dimensional frequency and buckling load parameters [5,27] are used

$$\mu = \frac{\omega a^2}{h}\sqrt{\frac{\rho_0}{E_0}},\ P_{cr}^* = P_{cr}\frac{a^2}{100h^3E_0}, \tag{32}$$

with ω is the fundamental frequency, and $E_0 = 1$ GPa, $\rho_0 = 1\ \mathrm{kg/m^3}$.

5.1. Convergence and accuracy studies

The convergence and accuracy of the derived element are firstly verified. To this end, the frequencies and buckling loads of (2-1-2) SSSS and CCCC BFGSW plates with $a/b = 2$ and $a/h = 10$ are computed using different meshes of the linked Q9 and a conventional (without linked interpolation) Mindlin Q9 element, and the results are shown in Fig. 5. Noting that, the Mindlin Q9 element differs only from linked Q9 element in which the interpolation for w uses the standard Lagrangian form, the same as u and v. As seen from the figure, convergence of the Linked Q9 is much faster than that of the conventional Q9 element, regardless of the B.C. and the power-law indexes. The convergence can be achieved by using 54 linked elements or a mesh of $3\times3\times6$. Regarding the computational cost, a mesh of 54 linked elements needs 3.196 s to get accurate fundamental frequency of the SSSS plate when a core i5 desktop with RAM 8G is used, while the corresponding time for a mesh of 96 conventional elements is 5.8847 s. Thus, the computational time can be improved significantly by using the linked element.

Since there is no data on the BFGSW plate in the literature, the accuracy of the derived Linked Q9 element is verified herewith by comparing the fundamental frequencies and buckling loads of unidirectional FGSW plate obtained herein with the published data. Table 2 presents the fundamental frequency and biaxial buckling load parameters of simply supported FGSW square plate with $a/h = 10$ of the present work with that of Refs. [5,7,13,27]. The sandwich plate in the references is a special case of the present BFGSW plate when $n_x = 0$. The maximum relative error of the parameters in Table 2, defined as $\mathrm{error}_{\max}(\%) = \dfrac{|\mathrm{result}_{\mathrm{present}} - \mathrm{result}_{\mathrm{reference}}|}{\mathrm{result}_{\mathrm{reference}}} \times 100\%$, is only 0.21 and 0.36% for the μ and P_{cr}^*, respectively. Thus, a good agreement between the frequencies and buckling loads of the present work with that of Ref. [5,7,13,27] can be noted from Table 2, regardless of the B.C. and the layer thickness ratio.

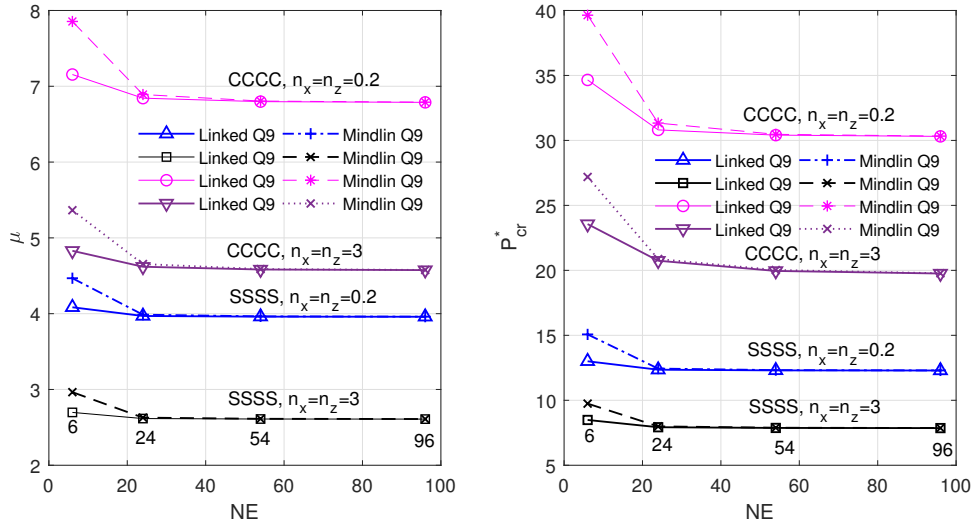

Fig. 5. A mesh convergence study for rectangular (2-1-2) BFGSW plates with $a/h = 10$

Table 2. Comparison of frequency and biaxial buckling load parameters of simply supported FGSW square plate with $a/h = 10$

	μ				P^*_{cr}			
n_z	Refs.	(2-1-2)	(1-1-1)	(1-2-1)	Refs.	(2-1-2)	(1-1-1)	(1-2-1)
0.5	Ref. [5]	1.4816	1.5170	1.5727	Ref. [5]	3.9566	4.2052	4.5976
	Ref. [13]	1.4841	1.5192	1.5745	Ref. [13]	3.9702	4.2181	4.6081
	Ref. [7]	1.4861	1.5213	1.5767	Ref. [27]	3.9707	4.2184	4.6083
	Present	1.4843	1.5195	1.5751	Present	3.9709	4.2190	4.6110
1	Ref. [5]	1.2973	1.3507	1.4372	Ref. [5]	2.9069	3.2195	3.7418
	Ref. [13]	1.3000	1.3533	1.4393	Ref. [13]	2.9193	3.2320	3.7528
	Ref. [7]	1.3018	1.3552	1.4414	Ref. [27]	2.9204	3.2326	3.7532
	Present	1.2991	1.3526	1.4391	Present	2.9147	3.2279	3.7512
5	Ref. [5]	0.9787	1.0418	1.1716	Ref. [5]	1.5113	1.7798	2.3574
	Ref. [13]	0.9796	1.0435	1.1735	Ref. [13]	1.5141	1.7855	2.3652
	Ref. [7]	0.9810	1.0453	1.1757	Ref. [27]	1.5218	1.7901	2.3674
	Present	0.9804	1.0436	1.1735	Present	1.5163	1.7858	2.3647

5.2. Parametric study

A rectangular BFGSW plate with $a/b = 2$ and various symmetric and non-symmetric thickness ratios and three values of the side-to-height, $a/h = 5$, $a/h = 20$ and $a/h = 100$, are considered in this subsection. The fundamental frequency and buckling load

parameters of the plate obtained by the derived element are given in Tables 3–8. The following remarks can be drawn from the tables.

Table 3. Frequency parameters of rectangular BFGSW plate with $a/h = 5$

n_x	n_z	SSSS			SCSC			CCCC		
		(2-1-2)	(1-1-1)	(2-2-1)	(2-1-2)	(1-1-1)	(2-2-1)	(2-1-2)	(1-1-1)	(2-2-1)
0.3	0.3	3.2249	3.2758	3.3131	3.3851	3.4374	3.4747	4.6164	4.6825	4.7229
	0.5	3.0261	3.1000	3.1558	3.1840	3.2602	3.3158	4.3885	4.4863	4.5463
	1	2.7021	2.8106	2.8982	2.8545	2.9672	3.0540	4.0053	4.1549	4.2479
	5	2.1512	2.2846	2.4315	2.2848	2.4280	2.5721	3.2782	3.5010	3.6552
0.5	0.3	3.2052	3.2593	3.2977	3.3634	3.4192	3.4578	4.5825	4.6538	4.6966
	0.5	3.0037	3.0809	3.1373	3.1588	3.2386	3.2952	4.3465	4.4501	4.5126
	1	2.6836	2.7936	2.8799	2.8321	2.9468	3.0328	3.9607	4.1144	4.2089
	5	2.1565	2.2886	2.4266	2.2855	2.4274	2.5639	3.2565	3.4773	3.6278
1	0.3	3.1693	3.2290	3.2693	3.3230	3.3849	3.4259	4.5214	4.6017	4.6486
	0.5	2.9634	3.0459	3.1035	3.1123	3.1982	3.2565	4.2724	4.3853	4.4520
	1	2.6492	2.7618	2.8460	2.7895	2.9074	2.9924	3.8833	4.0429	4.1396
	5	2.1558	2.2865	2.4120	2.2751	2.4160	2.5415	3.2132	3.4303	3.5746
5	0.3	3.0986	3.1681	3.2119	3.2423	3.3152	3.3604	4.4028	4.4983	4.5523
	0.5	2.8867	2.9778	3.0371	3.0227	3.1184	3.1795	4.1344	4.2613	4.3344
	1	2.5853	2.7009	2.7811	2.7093	2.8315	2.9137	3.7451	3.9113	4.0099
	5	2.1449	2.2735	2.3794	2.2455	2.3845	2.4929	3.1318	3.3395	3.4720

- The frequency parameter decreases by increasing the axial indexes n_x as well as the transverse index n_z. On the other hand, the buckling load parameter decreases by increasing the transverse index n_z while it increases by increasing the index n_x, regardless of the B.C., the layer thickness ratio and the side-to-height ratio. The influence of the power-law indexes on the buckling load can be explained by the change of the constituent percentage. As seen from Eq. (1), the percentage of M1 and M2 increases by the increase of n_x and n_z, and thus the rigidities of the plate increase, and this leads to the increase of the buckling load.

- The thickness ratio has a significant influence on the frequencies and buckling loads of the plate. The frequency and buckling load are higher for the plate associated with a larger core thickness. This is understandable since the core is made from high elastic modulus alumina, which results in a high stiffness plate.

- The frequency and buckling parameters are higher for the plate associated with a higher a/h ratio, regardless of the power-law indexes and the boundary conditions. The results in Tables 7 and 8 show the ability of the derived Q9 element in assessing the frequencies and buckling loads of the thin plate.

Table 4. Buckling load parameters of rectangular BFGSW plate with $a/h = 5$

n_x	n_z	SSSS			SCSC			CCCC		
		(2-1-2)	(1-1-1)	(2-2-1)	(2-1-2)	(1-1-1)	(2-2-1)	(2-1-2)	(1-1-1)	(2-2-1)
0.3	0.3	8.5918	8.8680	9.0688	9.3095	9.6049	9.8141	15.2290	15.6888	15.9749
	0.5	7.5711	7.9516	8.2378	8.2339	8.6419	8.9392	13.6858	14.3363	14.7447
	1	6.0317	6.5410	6.9550	6.6055	7.1546	7.5819	11.2573	12.1762	12.7685
	5	3.7494	4.2794	4.8651	4.1653	4.7498	5.3446	7.2302	8.3723	9.2163
0.5	0.3	8.7128	8.9757	9.1667	9.4384	9.7192	9.9180	15.3946	15.8349	16.1088
	0.5	7.7411	8.1044	8.3771	8.4169	8.8054	9.0882	13.9153	14.5411	14.9337
	1	6.2703	6.7596	7.1557	6.8677	7.3928	7.8003	11.5773	12.4673	13.0405
	5	4.0610	4.5845	5.1519	4.5241	5.0970	5.6699	7.6589	8.7906	9.6201
1	0.3	8.9254	9.1649	9.3385	9.6671	9.9218	10.1020	15.7046	16.1083	16.3590
	0.5	8.0405	8.3729	8.6217	8.7418	9.0954	9.3522	14.3452	14.9240	15.2866
	1	6.6925	7.1453	7.5090	7.3340	7.8157	8.1874	12.1770	13.0117	13.5479
	5	4.6219	5.1295	5.6622	5.1675	5.7160	6.2477	8.4623	9.5722	10.3709
5	0.3	9.3964	9.5805	9.7141	10.1682	10.3635	10.5016	16.4982	16.7926	16.9768
	0.5	8.7226	8.9770	9.1674	9.4660	9.7362	9.9323	15.5170	15.9384	16.2043
	1	7.7072	8.0516	8.3277	8.4073	8.7740	9.0564	13.9463	14.5654	14.9637
	5	6.1523	6.5526	6.9547	6.7798	7.2119	7.6160	11.0921	12.0271	12.6639

Table 5. Frequency parameters of rectangular BFGSW plate with $a/h = 20$

n_x	n_z	SSSS			SCSC			CCCC		
		(2-1-2)	(1-1-1)	(2-2-1)	(2-1-2)	(1-1-1)	(2-2-1)	(2-1-2)	(1-1-1)	
0.3	0.3	4.0014	4.0687	4.1225	4.4270	4.5006	4.5582	7.6205	7.7460	7.8389
	0.5	3.7198	3.8162	3.8956	4.1198	4.2254	4.3097	7.1052	7.2861	7.4202
	1	3.2728	3.4101	3.5321	3.6309	3.7819	3.9097	6.2793	6.5399	6.7377
	5	2.5607	2.7109	2.9059	2.8475	3.0146	3.2132	4.9336	5.2304	5.5191
0.5	0.3	3.9846	4.0556	4.1101	4.4075	4.4853	4.5439	7.5854	7.7182	7.8133
	0.5	3.7031	3.8031	3.8824	4.0999	4.2096	4.2943	7.0690	7.2570	7.3928
	1	3.2653	3.4042	3.5234	3.6204	3.7734	3.8991	6.2594	6.5232	6.7199
	5	2.5853	2.7348	2.9184	2.8711	3.0378	3.2263	4.9761	5.2709	5.5510
1	0.3	3.9524	4.0299	4.0859	4.3685	4.4539	4.5144	7.5208	7.6662	7.7651
	0.5	3.6705	3.7766	3.8560	4.0590	4.1761	4.2616	7.0027	7.2026	7.3409
	1	3.2465	3.3884	3.5033	3.5928	3.7498	3.8722	6.2198	6.4889	6.6834
	5	2.6118	2.7620	2.9286	2.8912	3.0593	3.2327	5.0282	5.3225	5.5885
5	0.3	3.8870	3.9764	4.0348	4.2873	4.3868	4.4511	7.3925	7.5604	7.6659
	0.5	3.6057	3.7224	3.8015	3.9758	4.1057	4.1923	6.8755	7.0950	7.2364
	1	3.2079	3.3544	3.4611	3.5350	3.6983	3.8141	6.1431	6.4199	6.6076
	5	2.6454	2.7982	2.9372	2.9087	3.0807	3.2294	5.0935	5.3907	5.6291

Table 6. Buckling load parameters of rectangular BFGSW plate with $a/h = 20$

n_x	n_z	SSSS			SCSC			CCCC		
		(2-1-2)	(1-1-1)	(2-2-1)	(2-1-2)	(1-1-1)	(2-2-1)	(2-1-2)	(1-1-1)	(2-2-1)
0.3	0.3	12.3967	12.8268	13.1738	14.6194	15.1242	15.5226	36.2553	37.5097	38.4498
	0.5	10.6840	11.2601	11.7422	12.6171	13.2934	13.8421	31.3278	33.0219	34.3022
	1	8.2155	8.9467	9.6140	9.7316	10.5897	11.3368	24.1350	26.3170	28.0225
	5	4.8994	5.5455	6.4131	5.8617	6.6196	7.5541	14.2519	16.2490	18.2591
0.5	0.3	12.6074	13.0170	13.3475	14.8686	15.3486	15.7279	36.8341	38.0329	38.9335
	0.5	10.9739	11.5240	11.9846	12.9631	13.6073	14.1311	32.1137	33.7403	34.9742
	1	8.6077	9.3107	9.9522	10.2084	11.0295	11.7464	25.1787	27.2913	28.9529
	5	5.3875	6.0215	6.8702	6.4810	7.2176	8.1275	15.5303	17.5026	19.5101
1	0.3	12.9782	13.3512	13.6525	15.3109	15.7465	16.0916	37.9226	39.0158	39.8409
	0.5	11.4862	11.9897	12.4116	13.5791	14.1656	14.6439	33.5978	35.0943	36.2374
	1	9.3079	9.9581	10.5518	11.0636	11.8162	12.4762	27.1676	29.1413	30.7110
	5	6.2839	6.8888	7.6956	7.6141	8.3053	9.1614	18.0258	19.9331	21.9116
5	0.3	13.7962	14.0841	14.3179	16.2767	16.6123	16.8799	40.5823	41.3850	42.0028
	0.5	12.6485	13.0355	13.3626	14.9469	15.3975	15.7690	37.4312	38.5211	39.3791
	1	10.9857	11.4808	11.9403	13.0249	13.6000	14.1142	32.7904	34.2183	35.4114
	5	8.7171	9.1682	9.7908	10.4185	10.9417	11.6146	26.1528	27.5794	29.1813

Table 7. Frequency parameters of rectangular BFGSW plate with $a/h = 100$

n_x	n_z	SSSS			SCSC			CCCC		
		(2-1-2)	(1-1-1)	(2-2-1)	(2-1-2)	(1-1-1)	(2-2-1)	(2-1-2)	(1-1-1)	(2-2-1)
0.3	0.3	4.0956	4.1648	4.2206	4.6804	4.7585	4.8198	8.2710	8.4104	8.5163
	0.5	3.8043	3.9034	3.9856	4.3535	4.4654	4.5549	7.6864	7.8861	8.0380
	1	3.3433	3.4840	3.6099	3.8349	3.9947	4.1296	6.7593	7.0440	7.2656
	5	2.6132	2.7657	2.9662	3.0082	3.1849	3.3925	5.2836	5.5961	5.9125
0.5	0.3	4.0792	4.1522	4.2087	4.6608	4.7433	4.8057	8.2376	8.3846	8.4926
	0.5	3.7883	3.8910	3.9731	4.3338	4.4501	4.5399	7.6538	7.8608	8.0141
	1	3.3371	3.4794	3.6024	3.8254	3.9872	4.1199	6.7468	7.0346	7.2546
	5	2.6397	2.7917	2.9804	3.0351	3.2113	3.4085	5.3411	5.6513	5.9585
1	0.3	4.0476	4.1273	4.1850	4.6215	4.7120	4.7763	8.1756	8.3358	8.4475
	0.5	3.7567	3.8657	3.9477	4.2930	4.4171	4.5077	7.5933	7.8128	7.9682
	1	3.3200	3.4654	3.5839	3.7994	3.9655	4.0948	6.7197	7.0128	7.2297
	5	2.6690	2.8218	2.9931	3.0601	3.2378	3.4195	5.4171	5.7271	6.0190
5	0.3	3.9831	4.0749	4.1350	4.5394	4.6448	4.7127	8.0518	8.2363	8.3539
	0.5	3.6935	3.8134	3.8948	4.2102	4.3477	4.4391	7.4770	7.7175	7.8749
	1	3.2842	3.4345	3.5444	3.7452	3.9179	4.0400	6.6668	6.9680	7.1762
	5	2.7068	2.8628	3.0058	3.0870	3.2685	3.4247	5.5234	5.8389	6.1007

Table 8. Buckling load parameters of rectangular BFGSW plate with $a/h = 100$

n_x	n_z	SSSS			SCSC			CCCC		
		(2-1-2)	(1-1-1)	(2-2-1)	(2-1-2)	(1-1-1)	(2-2-1)	(2-1-2)	(1-1-1)	(2-2-1)
0.3	0.3	12.8681	13.3167	13.6814	15.9406	16.4929	16.9299	40.9486	42.3868	43.4893
	0.5	11.0735	11.6728	12.1782	13.7466	14.4846	15.0840	35.2136	37.1375	38.6240
	1	8.4989	9.2558	9.9523	10.5994	11.5322	12.3430	26.9718	29.4078	31.3557
	5	5.0713	5.7319	6.6304	6.4098	7.2301	8.2329	15.9694	18.1118	20.3456
0.5	0.3	13.0904	13.5174	13.8648	16.2168	16.7416	17.1576	41.6511	43.0217	44.0761
	0.5	11.3793	11.9514	12.4341	14.1303	14.8327	15.4046	36.1753	38.0147	39.4437
	1	8.9133	9.6401	10.3094	11.1301	12.0208	12.7983	28.2663	30.6107	32.5021
	5	5.5913	6.2376	7.1151	7.1088	7.9015	8.8761	17.6004	19.6948	21.9187
1	0.3	13.4812	13.8700	14.1865	16.7093	17.1848	17.5628	42.9670	44.2099	45.1723
	0.5	11.9193	12.4424	12.8844	14.8165	15.4544	15.9762	37.9840	39.6620	40.9785
	1	9.6520	10.3229	10.9415	12.0845	12.8978	13.6123	30.7259	32.8876	34.6605
	5	6.5428	7.1559	7.9879	8.3893	9.1247	10.0379	20.7861	22.7637	24.9336
5	0.3	14.3394	14.6399	14.8860	17.7823	18.1476	18.4402	46.0475	46.9686	47.6966
	0.5	13.1351	13.5379	13.8814	16.3321	16.8210	17.2259	42.3734	43.6077	44.6087
	1	11.3982	11.9104	12.3910	14.2492	14.8687	15.4258	37.0807	38.6494	40.0131
	5	9.0562	9.5120	10.1572	11.4655	12.0173	12.7373	29.9665	31.3685	33.1068

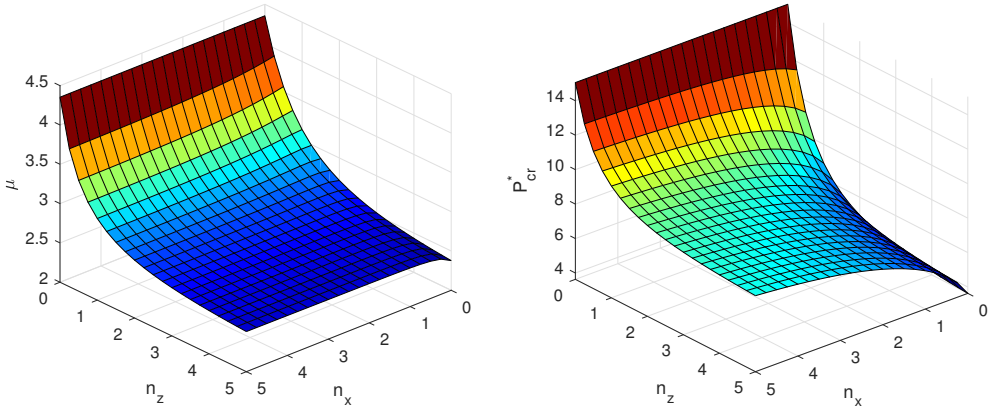

Fig. 6. Variation of frequency and buckling load parameters with power-law indexes of (2-1-2) BFGSW plates

The influence of the material distribution on the vibration and buckling behaviour of the BFGSW beam can also be seen clearly from Fig. 6, where the variation of the frequency and buckling load parameters with the power-law indexes is depicted for a rectangular symmetric (2-1-2) plate with $a/h = 10$. As can be seen from the figure, the influence of the transverse index n_z on the frequency and buckling load is more significant than

that of the axial index n_x. In addition, the influence of the index n_x on the vibration and buckling of the beam is more pronounced for $0 \leq n_z \leq 2$.

Finally, the effect of the side-to-thickness ratio a/h on the fundamental frequency and buckling load of the BFGSW plate is studied. To this end, Fig. 7 shows the dependence of the frequency and buckling parameters on the side-to-thickness ratio of a symmetric (2-1-2) rectangular plate with different boundary conditions and power-law indexes. The frequency and buckling load parameters steadily increase by increasing the aspect ratio, and the increase is the most significant for a/h smaller 20, regardless of the boundary conditions and the power-law indexes.

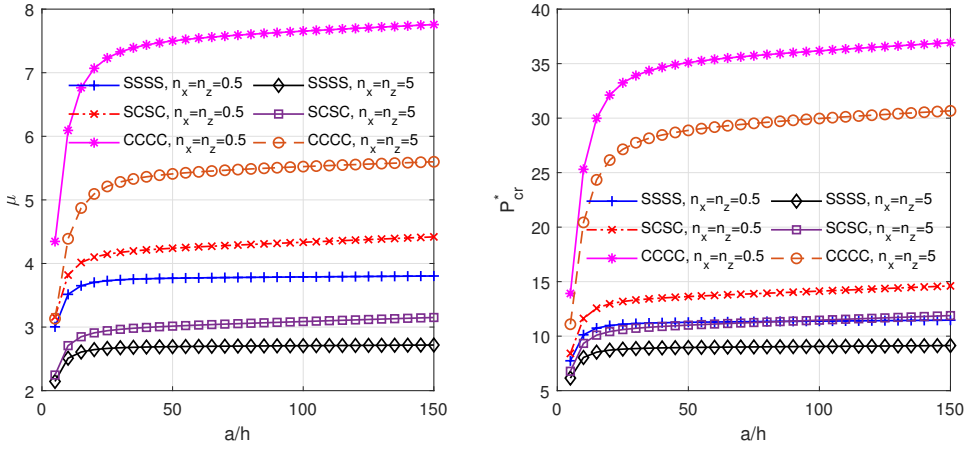

Fig. 7. Dependence of frequency and buckling load parameters on side-to-thickness ratio of (2-1-2) BFGSW plate

6. CONCLUSIONS

A Q9 element has been formulated and used in computing natural frequencies and buckling loads of BFGSW rectangular plates. The core of the sandwich plates is pure ceramic, while the face layers are of three-phase BFGM. The efficiency of the element has been improved by using the linked interpolations. The numerical investigation shows that the linked Q9 is accurate and its convergence element is faster compared to the conventional Q9 element. Using the derived element, fundamental frequencies and buckling loads of BFGSW rectangular plates have been computed, and the effects of the material distribution and plate geometry have been studied in detail and highlighted.

REFERENCES

[1] V. Birman and L. W. Byrd. Modeling and analysis of functionally graded materials and structures. *Applied Mechanics Reviews*, **60**, (5), (2007), pp. 195–216. https://doi.org/10.1115/1.2777164.

[2] K. Swaminathan, D. T. Naveenkumar, A. M. Zenkour, and E. Carrera. Stress, vibration and buckling analyses of FGM plates-A state-of-the-art review. *Composite Structures*, **120**, (2015), pp. 10–31. https://doi.org/10.1016/j.compstruct.2014.09.070.

[3] Y. Fukui. Fundamental investigation of functionally gradient material manufacturing system using centrifugal force. *Japan Society of Mechanical Engineering International Journal, Series III: Vibration, Control Engineering, Engineering for Industry*, **34**, (1), (1991), pp. 144–148. https://doi.org/10.1299/jsmec1988.34.144.

[4] A. M. Zenkour. A comprehensive analysis of functionally graded sandwich plates: Part 1—Deflection and stresses. *International Journal of Solids and Structures*, **42**, (2005), pp. 5224–5242. https://doi.org/10.1016/j.ijsolstr.2005.02.015.

[5] A. M. Zenkour. A comprehensive analysis of functionally graded sandwich plates: Part 2—Buckling and free vibration. *International Journal of Solids and Structures*, **42**, (2005), pp. 5243–5258. https://doi.org/10.1016/j.ijsolstr.2005.02.016.

[6] A. M. Zenkour and M. Sobhy. Thermal buckling of various types of FGM sandwich plates. *Composite Structures*, **93**, (2010), pp. 93–102. https://doi.org/10.1016/j.compstruct.2010.06.012.

[7] Q. Li, V. P. Iu, and K. P. Kou. Three-dimensional vibration analysis of functionally graded material sandwich plates. *Journal of Sound and Vibration*, **311**, (1–2), (2008), pp. 498–515. https://doi.org/10.1016/j.jsv.2007.09.018.

[8] S. Xiang, Y. X. Jin, Z. Y. Bi, S. X. Jiang, and M. S. Yang. A *n*-order shear deformation theory for free vibration of functionally graded and composite sandwich plates. *Composite Structures*, **93**, (11), (2011), pp. 2826–2832. https://doi.org/10.1016/j.compstruct.2011.05.022.

[9] S. Xiang, G. W. Kang, M. S. Yang, and Y. Zhao. Natural frequencies of sandwich plate with functionally graded face and homogeneous core. *Composite Structures*, **96**, (2013), pp. 226–231. https://doi.org/10.1016/j.compstruct.2012.09.003.

[10] A. M. A. Neves, A. J. M. Ferreira, E. Carrera, M. Cinefra, C. M. C. Roque, R. M. N. Jorge, and C. M. Soares. Static, free vibration and buckling analysis of isotropic and sandwich functionally graded plates using a quasi-3D higher-order shear deformation theory and a meshless technique. *Composites Part B: Engineering*, **44**, (1), (2013), pp. 657–674. https://doi.org/10.1016/j.compositesb.2012.01.089.

[11] H. T. Thai and D. H. Choi. Finite element formulation of various four unknown shear deformation theories for functionally graded plates. *Finite Elements in Analysis and Design*, **75**, (2013), pp. 50–61. https://doi.org/10.1016/j.finel.2013.07.003.

[12] H. T. Thai and S. E. Kim. A simple higher-order shear deformation theory for bending and free vibration analysis of functionally graded plates. *Composite Structures*, **96**, (2013), pp. 165–173. https://doi.org/10.1016/j.compstruct.2012.08.025.

[13] H. T. Thai, T. K. Nguyen, T. P. Vo, and J. Lee. Analysis of functionally graded sandwich plates using a new first-order shear deformation theory. *European Journal of Mechanics-A/Solids*, **45**, (2014), pp. 211–225. https://doi.org/10.1016/j.euromechsol.2013.12.008.

[14] L. Iurlaro, M. Gherlone, and M. DiSciuva. Bending and free vibration analysis of functionally graded sandwich plates using the refined zigzag theory. *Journal of Sandwich Structures & Materials*, **16**, (6), (2014), pp. 669–699. https://doi.org/10.1177/1099636214548618.

[15] S. Pandey and S. Pradyumna. Analysis of functionally graded sandwich plates using a higher-order layerwise theory. *Composites Part B: Engineering*, **153**, (2018), pp. 325–336. https://doi.org/10.1016/j.compositesb.2018.08.121.

[16] Z. Belabed, A. A. Bousahla, M. S. A. Houari, A. Tounsi, and S. R. Mahmoud. A new 3-unknown hyperbolic shear deformation theory for vibration of functionally graded sandwich plate. *Earthquakes and Structures*, **14**, (2), (2018), pp. 103–115. https://doi.org/10.12989/eas.2018.14.2.103.

[17] A. A. Daikh and A. M. Zenkour. Effect of porosity on the bending analysis of various functionally graded sandwich plates. *Materials Research Express*, **6**, (6), (2019). https://doi.org/10.1088/2053-1591/ab0971.

[18] C. I. Le, V. N. Pham, and D. K. Nguyen. Free vibration of FG sandwich plates partially supported by elastic foundation using a quasi-3D finite element formulation. *Vietnam Journal of Mechanics*, **42**, (1), (2020), pp. 63–86. https://doi.org/10.15625/0866-7136/14701.

[19] P. S. Ghatage, V. R. Kar, and P. E. Sudhagar. On the numerical modelling and analysis of multi-directional functionally graded composite structures: A review. *Composite Structures*, **236**, (2020). https://doi.org/10.1016/j.compstruct.2019.111837.

[20] O. C. Zienkiewicz, Z. Xu, L. F. Zeng, A. Samuelsson, and N.-E. Wiberg. Linked interpolation for Reissner-Mindlin plate elements: Part I—A simple quadrilateral. *International Journal for Numerical Methods in Engineering*, **36**, (1993), pp. 3043–3056. https://doi.org/10.1002/nme.1620361802.

[21] R. L. Taylor and F. Auricchio. Linked interpolation for Reissner-Mindlin plate elements: Part II—A simple triangle. *International Journal for Numerical Methods in Engineering*, **36**, (1993), pp. 3057–3066. https://doi.org/10.1002/nme.1620361803.

[22] Z. Xu, O. C. Zienkiewicz, and L. F. Zeng. Linked interpolation for Reissner-Mindlin plate elements: Part III—An alternative quadrilateral. *International Journal for Numerical Methods in Engineering*, **37**, (1994), pp. 1437–1443. https://doi.org/10.1002/nme.1620370902.

[23] D. Ribarić and G. Jelenić. Higher-order linked interpolation in quadrilateral thick plate finite elements. *Finite Elements in Analysis and Design*, **51**, (2012), pp. 67–80. https://doi.org/10.1016/j.finel.2011.10.003.

[24] D. Ribarić and G. Jelenić. Higher-order linked interpolation in triangular thick plate finite elements. *Engineering Computations*, **31**, (2014), pp. 69–109. https://doi.org/10.1108/ec-03-2012-0056.

[25] M. Nemat-Alla, K. I. Ahmed, and I. Hassab-Allah. Elastic–plastic analysis of two-dimensional functionally graded materials under thermal loading. *International Journal of Solids and Structures*, **46**, (2009), pp. 2774–2786. https://doi.org/10.1016/j.ijsolstr.2009.03.008.

[26] D. K. Nguyen, T. T. Tran, V. N. Pham, and N. A. T. Le. Dynamic analysis of an inclined sandwich beam with bidirectional functionally graded face sheets under a moving mass. *European Journal of Mechanics/A Solids*, **88**, (2021). https://doi.org/10.1016/j.euromechsol.2021.104276.

[27] S. S. Akavci. Mechanical behavior of functionally graded sandwich plates on elastic foundation. *Composites Part B: Engineering*, **96**, (2016), pp. 136–152. https://doi.org/10.1016/j.compositesb.2016.04.035.

[28] O. C. Zienkiewicz and R. L. Taylor. *The Finite Element Method, volume 2: Solid Mechanics*. Butterworth - Heinemann, (2020).